

Compositional and metal-insulator transition characteristics of sputtered vanadium oxide thin films on yttria-stabilized zirconia

Gokul Gopalakrishnan · Shriram Ramanathan

Received: 25 October 2010 / Accepted: 4 April 2011 / Published online: 21 April 2011
© Springer Science+Business Media, LLC 2011

Abstract Vanadium dioxide (VO_2) thin films have been shown to undergo a rapid electronic phase transition near 70°C from a semiconductor to a metal, making it an interesting candidate for exploring potential application in high speed electronic devices such as optical switches, tunable capacitors, and field effect transistors. A critical aspect of lithographic fabrication in devices utilizing electric field effects in VO_2 is the ability to grow VO_2 over thin dielectric films. In this article, we study the properties of VO_2 grown on thin films of Yttria-Stabilized Zirconia (YSZ). Near room temperature, YSZ is a good insulator with a high dielectric constant ($\epsilon_r > 25$). We demonstrate the sputter growth of polycrystalline VO_2 on YSZ thin films, showing a three order resistivity transition near 70°C with transition and hysteresis widths of approximately 7°C each. We examine the relationship between chemical composition and transition characteristics of mixed phase vanadium oxide films. We investigate changes in composition induced by low temperature post-deposition annealing in oxidizing and reducing atmospheres, and report their effects on electronic properties.

Introduction

Investigations into the behavior of a wide range of correlated transition metal oxides and the simultaneous maturation of thin film growth technology have resulted in renewed attention to the properties of complex oxides,

from not only a scientific perspective but also towards their use in novel electronic devices. One such material, vanadium dioxide (VO_2), has been shown to undergo a structural phase transition [1, 2] (SPT) at about 70°C , that is closely accompanied by an abrupt resistance change from a metal-insulator transition (MIT) [3, 4]. This ultra-fast transition [5] in VO_2 near room temperature has made it the focus of intensive experimental and theoretical research in recent years.

The scientific interest in VO_2 is driven largely by the origin of the MIT in VO_2 , which is still under debate. Within the Peierls picture [2], the structural phase transition between a low temperature monoclinic phase and a high temperature tetragonal phase involves a doubling of the unit cell, which leads to a closing of the band gap. However, this picture can not easily explain recent experiments [6, 7], such as those that demonstrate a voltage-induced conductance change over timescales smaller than thermal transport times [8]. An alternative model based on a Mott transition overcomes many of these difficulties. Within this picture, the insulating state is characterized by an energy gap that arises from electron-electron interactions, and is a function of carrier density. At a critical density, the gap vanishes, leading to a transition to the metallic state [9].

To help distinguish between the two mechanisms, it is of great interest to investigate whether a static electric field can be used to generate the carrier density needed to trigger the transition in accordance with the Mott picture. In two terminal structures, VO_2 thin films have been observed to exhibit a similar transition when an electric field on the order of 10^6V/m is induced in it [9–12]. However, due to filamentary currents that may flow in the high resistance state, the magnitude of local Joule heat-induced temperature changes [15–17] in these devices leaves some room for

G. Gopalakrishnan (✉) · S. Ramanathan
School of Engineering and Applied Sciences, Harvard
University, Cambridge, MA 02138, USA
e-mail: gokul@seas.harvard.edu

doubt about the underlying mechanism. It is therefore important to this line of inquiry to be able to investigate field effects in devices with minimal leakage, including, for instance, capacitors and gated structures.

Growth of VO_2 on dielectric materials like Al_2O_3 , SiO_2 , and HfO_2 has been explored in previous studies [9, 13, 14, 19]. In this article, we study the sputter deposition of vanadium oxide on Yttria-Stabilized Zirconia (YSZ), an oxide which is extremely stable under the typical growth conditions for VO_2 . YSZ thin films have been shown to have properties that are advantageous for their use as an insulator in capacitors and gated field effect devices: notably, a high dielectric constant and low leakage near room temperature [20]. Recent study by Gupta et al. [18] demonstrates the growth of epitaxial VO_2 by laser ablation on Si(001) with a 200 nm thick buffer layer of epitaxial YSZ, showing a large resistance transition of three orders of magnitude and hysteresis and transition widths smaller than 8 K. Our study is devoted to sputter deposition over untextured YSZ films as thin as 25 nm, and we report successful growth of polycrystalline films with transition characteristics similar to those achieved by epitaxial growth.

The temperature-dependent resistivity of vanadium oxide measured in these films shows a strong transition near 70 °C, which is close to the value for single crystals and about 10 °C lower than that measured in the strained epitaxial films of Gupta et al. [18]. While sputtering under carefully optimized conditions can yield films with a high concentration of VO_2 , it is typical for higher and lower oxides [22], primarily V_2O_5 and V_2O_3 to be present, which influence the quality of this transition. We study the role of these phases on the transition characteristics and examine the changes in composition as a function of annealing. While previous studies have investigated post-deposition annealing at low pressures or temperatures above the growth temperature, in this study we report on the compositional changes in mixed phase films induced by annealing within a relatively unexplored regime of low temperatures at atmospheric pressure, and attendant changes in the transition characteristics.

Experiment

We describe the growth of vanadium oxide over YSZ on two different substrates: *c*-plane sapphire (*c*- Al_2O_3) and *n*-type As-doped Si (resistivity = 2–5 $\Omega^{-\text{cm}}$). A third substrate, $\text{Si}/\text{Si}_3\text{N}_4$ is also found to be suitable for growth of VO_2/YSZ with similar properties. A 25-nm thick layer of YSZ was deposited by RF sputtering in an AJA International ATC series sputtering chamber, from a

ceramic target. The sample temperature was 550 °C during the growth in an Ar atmosphere at a pressure of 5 mTorr. Vanadium oxide (VO_x) thin films were then grown over the YSZ layer by either DC or RF sputtering, also at a temperature of 550 °C. DC reactive sputtering from a vanadium target was performed in an atmosphere of O_2 and Ar at a combined flow rate of 100 sccm and a total pressure of 10 mTorr. VO_x films grown over 75 min at a power of 250 W were measured to be approximately 150 nm thick. RF-sputtered films of similar thickness were grown from a ceramic VO_2 target at a power of 150 W over 180 min. While DC sputtering typically requires about 10% O_2 to grow films with average composition near VO_2 , the fraction for RF sputtering is close to 2.5% O_2 .

The surface roughness and grain size were estimated by Atomic Force Microscopy (AFM) on an Asylum MFP-3D system. The presence of the VO_2 phase in all the films was confirmed by X-Ray Diffraction (XRD) on a Bruker AXS diffractometer, using a beam of Cu K_α radiation at a fixed glancing incidence of 2°. X-Ray Photoelectron Spectroscopy (XPS) with Al K_α radiation, using a XXS-100 ESCA Spectrometer was employed to examine the composition of the films. Since the detected photoelectrons provide information about only the top 1–2 nm, an in-situ Ar plasma was used to etch into the film, for the purpose of studying variations in composition as a function of depth into the film. Relative ratios of V to O are estimated by scaling the areas under peaks with the Relative Sensitivity Factor (RSF) of the species, after subtraction of a Shirley background.

Two-probe resistance and capacitance measurements on VO_2 films were performed using an MDC Systems environmental probe station. *I*–*V* curves measured by a Keithley-236 source-meter within the Ohmic regime were used to determine film resistance between a pair of tungsten probes making contact with the bare VO_2 surface. While the measured resistance was found to vary weakly with probe separation (maintained at approximately 3 mm) and location on the film (fixed roughly by markers), the normalized resistance, $\mathcal{R}_T = R(T)/R(100^\circ\text{C})$, was determined to be a robust characteristic of the film. For *C*–*V* measurements, top gate electrodes of Cr–Au were thermally evaporated onto samples with *n*-Si substrate, with the substrate serving as the bottom electrode.

The as-grown films, after characterization, were subjected to a series of annealing steps. Sample B ($\text{VO}_2/\text{YSZ}/\text{n-Si}$) was annealed in air for 90 min each, at temperatures successively rising from 100 to 300 °C. Sample A ($\text{VO}_2/\text{YSZ}/\text{c-Al}_2\text{O}_3$) was similarly annealed at increasing temperatures, in a reducing atmosphere of 5% H_2 in Ar. Properties of the samples were measured after each stage of annealing.

Results and Discussion

The YSZ films sputtered at 550 °C are found to be crystalline but with no particular texture, as confirmed by XRD measurements (see Fig. 1). Over the course of this article, we describe the structure, composition, and transition characteristics of three vanadium oxide thin films: sample X is an RF-sputtered film on YSZ/n-Si, while samples A and B are DC-sputtered films grown together over a YSZ layer, with *c*-Al₂O₃ and *n*-Si substrates, respectively. The DC-sputtered films have a relatively large value of the root-mean-square roughness of about 40 nm, and a correspondingly large grain size near 100 nm, estimated from AFM scans of the surface. These films are not optimized for growth of VO₂ and contain significant fractions of other oxide phases. A and B are therefore used to study the changes in these phases and their effect on transition characteristics, over a series of annealing steps.

Sample X is an example of an RF-sputtered film showing a large transition order, defined here as $\mathcal{R}_{tr} = R(50^{\circ}\text{C})/R(100^{\circ}\text{C})$. The film thickness is approximately 150 nm and the surface roughness is smaller than 10 nm. Figure 1 shows a GIXRD measurement of this sample with a small region of the underlying YSZ exposed to the beam. The positions of the strongest reflections for VO₂ are indicated, and we identify peaks corresponding to several of them. We also observe the two strongest Bragg peaks from the partially exposed YSZ layer. As is typical for RF-sputtered VO₂, this film is seen to have a significantly smaller grain size than those of the DC-sputtered films. The estimate of mean grain size for sample X, deduced from the width of XRD peaks via the Scherrer formula, is roughly 10 nm.

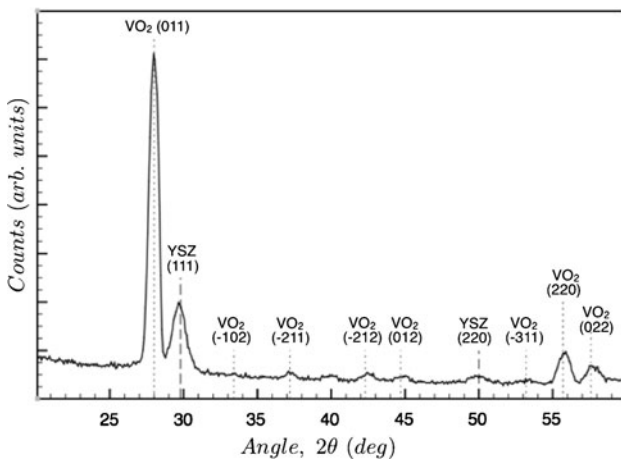


Fig. 1 GIXRD scan for sample B (VO₂/YSZ/*n*-Si) over an area of film with a region of partially exposed YSZ. 2θ values for prominent Bragg reflections in monoclinic VO₂ and YSZ are indicated via dashed lines and labeled accordingly

Vanadium oxide films grown simultaneously over the YSZ layer are found to have similar temperature dependence of resistance, irrespective of the substrate. Figure 2 shows the normalized resistance of the three samples. Between A and B, there are some small variations in the transition temperature and hysteresis width, but the order of the transition, \mathcal{R}_{tr} , is nearly identical for these films.

RF-sputtered sample X is nearly optimized for VO₂ growth and shows a large \mathcal{R}_{tr} of about 10³. The transition width, estimated from a Gaussian fit to the derivative, $\delta(\log \mathcal{R})/\delta T$, is also close to 7 °C. These characteristics of the polycrystalline film in sample X are nearly identical to those of epitaxial VO₂/YSZ described in Ref. [18]. A notable difference in the transition behavior, however, is in the transition temperature itself. The epitaxial films in Ref. [18] have a transition during heating near 80 °C, which is about 10 °C higher than the typical single crystal value. Gupta et al. attribute this difference to a tensile strain in the *c*-direction. Sample X, being nanocrystalline, is relatively free of such strain, and exhibits a transition close to the typical bulk value. Nevertheless, the hysteresis width of approximately 7 °C in our sample X is about the same as that of the epitaxially grown film.

Samples A and B, and to a lesser extent, sample X, show the existence of multiple oxide phases, as is often the case in sputtered vanadium oxide films. The presence of additional phases contributes to a reduction in the transition order compared to pure VO₂ ($\mathcal{R}_{tr} \sim 10^4$). Moreover, while single phase VO₂ has been reported [11] to exhibit activated transport ($R(T) = R_0 e^{\epsilon/kT}$) with an activation energy of about 0.2 eV, all three samples produce very similar Arrhenius plots (Fig. 2a) with activation energies of 0.1 eV.

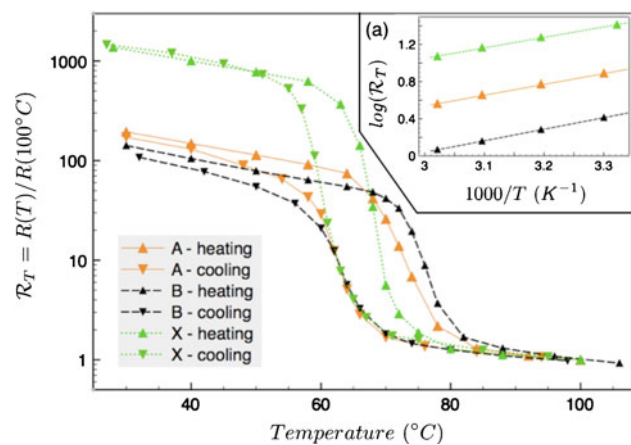


Fig. 2 Heating and cooling curves of \mathcal{R}_T for samples A, B, and X, showing a transition order of $\mathcal{R}_{tr} \approx 10^2$ for DC-sputtered samples A and B, and $\mathcal{R}_{tr} \approx 10^3$ for RF-sputtered sample X. Inset a Arrhenius plots (with arbitrary offsets) show nearly identical activation energies of approximately 0.1 eV for all three samples

The coexistence of multiple oxidation states is also seen in XPS measurements. While a scan of the surface shows small peaks from carbon and nitrogen, due to organic contamination, these peaks vanish after a 5-min cleaning in Ar plasma. Figure 3 shows a series of XPS scans on as-grown sample A, as a function of depth into the VO_x film. The largest available beam size (1 mm) is used, to average over microscopic inhomogeneities along directions normal to the film thickness. The primary features displayed are two peaks corresponding to the V- $2P$ ($2P_{3/2}$ and $2P_{1/2}$) states and one peak from O-1S.

As depth into the films increases, the separation between the V- $2P_{3/2}$ and O-1S peaks is observed to increase. This variation, seen in multiple samples, is interpreted as a decrease in oxygen content away from the surface, as individual peaks for V^{3+} , V^{4+} , and V^{5+} are reported to occur at closely separated but successively increasing binding energies (BE) [21–25]. The V- $2P_{3/2}$ peak is assumed to be a convolution of these three peaks, as reported in previous literature, [21, 22, 25] and a systematic variation in the relative fractions of the components gives rise to a corresponding shift in the peak position of their envelope. This behavior is also consistent with trends in the ratio of areas under the V- $2P_{3/2}$ and O-1S peaks. Compositions estimated by scaling the areas under the V and O peaks by their RSF suggest an average stoichiometry of approximately $\text{VO}_{2.2}$ at the surface, and about $\text{VO}_{1.8}$ at a depth of 60 nm. The depth variation in the BE difference between the V- $2P_{3/2}$ and O-1S peaks is well fit by an exponential decay, as shown in Fig. 3a, with a decay length scale of approximately 14 nm. This observation of a depth-dependent stoichiometry with the surface richer in oxygen

than the interior of the film is seen in multiple sputtered films.

The characterized as-grown samples were then subjected to a series of anneals, as described in the “Experiment” section above. Much previous literature on annealing of vanadium oxide thin films relates to annealing temperatures in the vicinity of 500 °C. Also, Yun et al. [27] report on the chemical reduction of the VO_2 phase at temperatures as low as 200 °C under vacuum annealing. The scope of our study is to examine the effect of annealing at atmospheric pressure and at low temperatures, not far from the transition temperature itself. Not only does this explore a range of annealing conditions that have not seen much previous investigation, it is also important from the point of view of examining the potential for device deterioration under common working conditions that involve heating above the transition temperature.

Figures 4 and 5 show changes in the transition characteristics as a function of annealing temperature. We find that there is no detectable change in \mathcal{R}_T from annealing for 90 minutes at 100 °C, in the case of both the samples A and B. This is significant, as the process of inducing or measuring the thermal transition necessarily involves heating the sample through temperatures up to about 100 °C. Figure 4 shows \mathcal{R}_T curves for sample B, demonstrating a significant lowering of \mathcal{R}_{tr} after annealing in air at only 150 °C. Subsequent anneals at higher temperatures cause incremental reductions in the transition order with a weak downward trend in the transition temperature. For sample A, annealed in forming gas (5% H₂ in Ar), measurable changes in the transition are observed near 200 °C, as seen in Fig. 5, with a large deterioration of the transition order observed beyond 300 °C. In both samples, there is no significant change observed in the width of hysteresis,

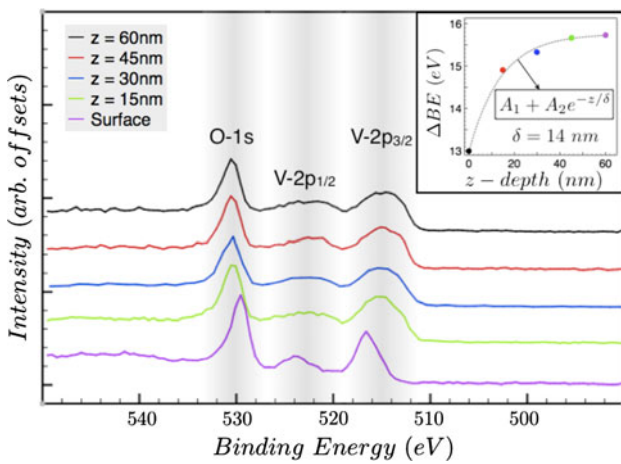


Fig. 3 XPS depth profile showing V- $2P_{3/2}$, V- $2P_{1/2}$ and O-1S peaks as a function of depth into the film. Inset variation in BE differences between V- $2P_{3/2}$ and O-1S peaks is observed to saturate near 15.8 eV, and is well fit by an exponential curve with a decay length of $\delta = 14$ nm

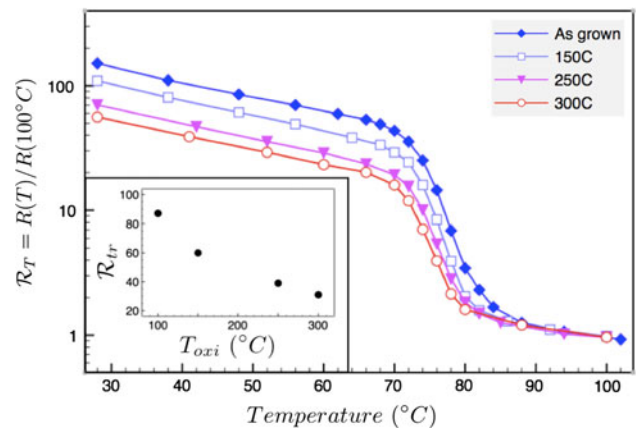


Fig. 4 Temperature dependence of normalized resistance \mathcal{R}_T , after each stage of a series of oxidizing anneals, performed on sample B in air. Inset shows the variation of the transition order \mathcal{R}_{tr} , as a function of the anneal temperature

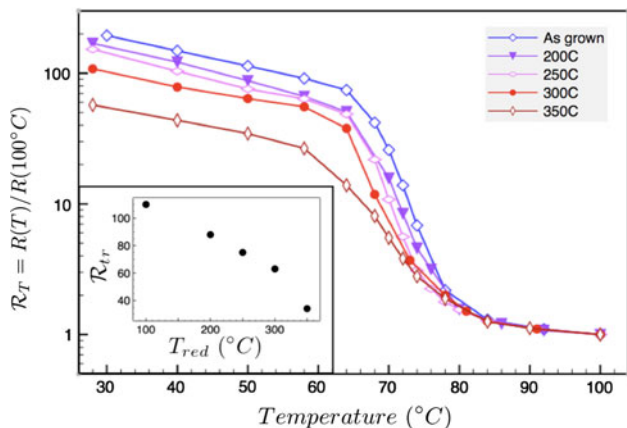


Fig. 5 Temperature dependence of normalized resistance R_T , after each stage of a series of reducing anneals performed on sample A in forming gas. Inset shows the variation of transition order R_{tr} , as a function of the anneal temperature

which is consistent with AFM measurements showing similar grain sizes before and after annealing.

These changes in resistivity are compared with changes in the XPS spectra. Depth profiles after annealing continue to show a film surface that is somewhat oxygen rich compared to the bulk. In Sample B, the relative positions of the V- $2P_{3/2}$ and O-1S peaks shift towards each other after annealing in air, and with sample A, they move away from each other after the annealing in forming gas. This is consistent with the expectation of oxidation or reduction from the respective anneals, due to the trends in the binding energies of different oxidation states. Furthermore, high resolution scans of the V- $2P_{3/2}$ peak indicate changes in the line shape, which we attempt to resolve via deconvolution of the composite peak into its three most dominant components, after subtraction of a Shirley background. This procedure may only be useful for a qualitative, or at best, approximately quantitative understanding, due to the closeness of the peak positions for different oxidation states.

In Fig. 6, we compare the line shapes of the V- $2P_{3/2}$ peaks in sample B measured at a depth of 30 nm before and after the sequence of oxidizing anneals. We identify three dominant components of the deconvolution, labeled V_3 , V_4 , and V_5 . We attribute this structure to the significant presence of V^{3+} , V^{4+} , and V^{5+} peaks in the V- $2P_{3/2}$ envelope, with BEs increasing with the oxidation state, as expected from the change in the number of d -electrons. We note that the energy difference between these components is somewhat larger than values typically reported in literature [22–25] for the respective oxidation states. We therefore do not rule out the possibility of additional phases (from V^{2+} , for example) contributing to the deconvolution. Using this deconvolution to provide an approximation of the relative presence of these components, we find that the effect of the oxidizing anneal indicates some conversion of

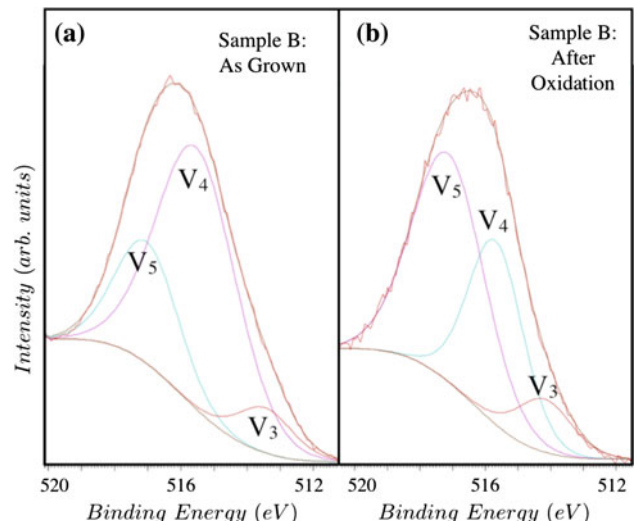


Fig. 6 Deconvolution of the V- $2P_{3/2}$ peaks in XPS spectra of sample B at a depth of 30 nm below the surface, **a** as grown and **b** after oxidizing anneal at 300°C

VO_2 to higher oxide phases like V_2O_5 , but no significant change in the fraction of the low oxidation phases like V_2O_3 .

Figure 7 provides a similar comparison for sample A, before and after the annealing sequence in reducing environment. We interpret the constancy in the V_5 peak of the three component deconvolution as indicating no significant change in the high oxidation phases. While there is a reduction in area under the V_4 component, we do not see an attendant increase in peak labeled V_3 . Instead we find that the best three component fit now involves a new component, V_{γ} , significantly closer in energy to V_4 . We interpret this change in the deconvolution as suggesting the possible emergence one or more of the V_4O_7 and V_3O_5 phases known to exist in mixed phase vanadium oxide films above room temperature. This interpretation is consistent with vacuum reduction results reported by Yun et al. [27], showing a degradation of the VO_2 phase at 200°C , but with no accompanying increase in the V_2O_3 phase until about 550°C .

One test of our interpretation of the deconvolution is to compare estimates of the average stoichiometry based on the ratios of these three components with values determined from the ratio of areas under V and O peaks. We find reasonable agreement between these two estimates. For instance, the RSF-scaled areas for fully annealed sample B at a depth of 30 nm are in the ratio of $\text{V} \approx 32\%$ to $\text{O} \approx 68\%$, giving a mean composition of $\text{VO}_{2.13}$. On the other hand, the areas under the V^{3+} , V^{4+} , and V^{5+} peaks in the deconvolution of Fig. 5b provide the ratios of $\text{V}_2\text{O}_3 \sim 10\%$, $\text{VO}_2 \sim 35\%$, and $\text{V}_2\text{O}_5 \sim 55\%$, yielding an estimate for the aggregate composition of $\text{VO}_{2.18}$.

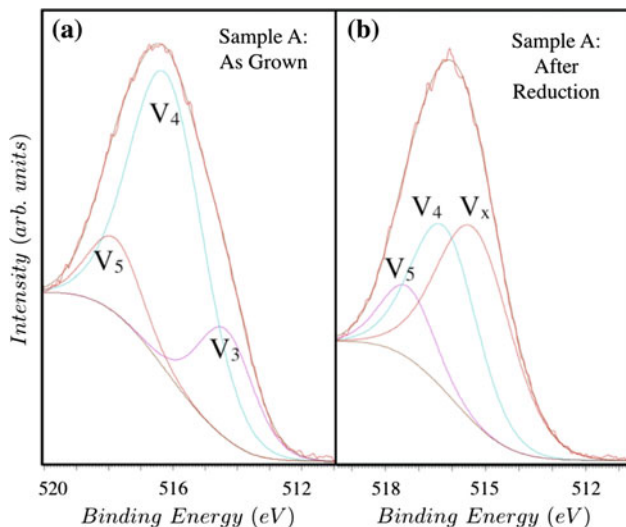


Fig. 7 Deconvolution of the V-2P_{3/2} peaks in XPS spectra of sample A at a depth of 30 nm below the surface, **a** as grown and **b** after final reducing anneal at 350 °C

The nature of the composition changes resulting from the annealing sequences are notable. Samples with similar starting compositions were subjected to different annealing conditions, sample A annealed in forming gas and sample B in air. The changes in the overall stoichiometry, confirmed by the XPS measurements, are consistent with the expectation that some oxidation occurs in sample B and reduction in sample A. Nevertheless, both treatments resulted in a net degradation of the transition order. This is explained in the case of sample A as arising from a reduction of the VO₂ phase, with V₂O₅ and other high oxidation phases unchanged. For sample B, we attribute the degradation to an oxidation of VO₂, with no significant contribution to the VO₂ fraction from the oxidation of lower oxide phases. In both cases, it is notable that the most reactive phase of significant presence is interpreted as being the VO₂ phase, while higher and lower oxygen phases appear to be more stable under the conditions explored.

Annealed sample B was retained for studying C-V characteristics. After depositing a top gate electrode of Cr–Au, a series of C-V curves were measured in the range of -2 to 2 V at a frequency of 1 MHz, using a ramp rate of approximately 0.05 V/s. While leakage currents on the order of 10⁻⁶ A/cm² were measured at ±2 V on Au–Cr/YSZ/n-Si, larger leakage of about 10⁻² A/cm² is measured in Au–Cr/VO_x/YSZ/n-Si which is due to the unpatterned vanadium oxide layer providing a conductive channel to remote regions, such as sample edges, where the YSZ is not as leak-tight.

Figure 8 displays the overall temperature dependence of the capacitance at zero bias, showing an abrupt increase in

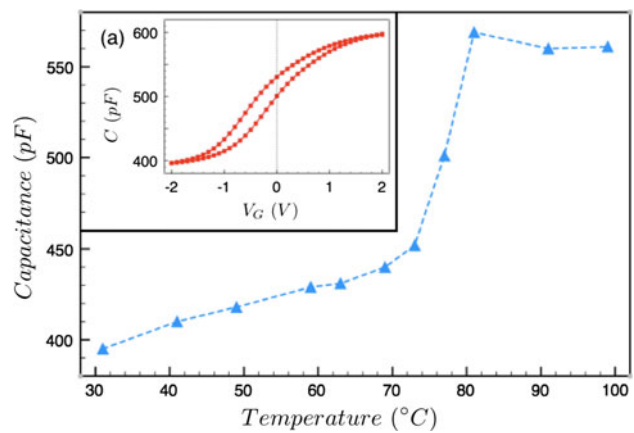


Fig. 8 Temperature dependence of total capacitance at $V_G = 0$ V, showing a significant increase near the transition temperature. *Inset a* a representative C-V plot measured at 77 °C, showing behavior characteristic of inversion near -2 V and accumulation near +2 V, with a regime of depletion in between

capacitance over the same range of temperatures as the resistivity transition measured during heating (compare with Fig. 2). This increase is explained as a consequence of the vanadium oxide layer turning metallic near the transition temperature, thereby reducing the effective thickness of the capacitor. Similar increases are observed across the transition for capacitance values in the regions typically associated with inversion and accumulation. This temperature dependence suggests that the vanadium oxide layer contributes to values of both the oxide capacitance, C_{ox} , as well as the semiconductor capacitance, C_s (within the standard MOS capacitor description). Inset 8a shows a representative C-V curve measured at 77 °C. All measured C-V plots exhibit the typical sigmoidal shape similar to that of a MOS capacitor measured in the high frequency limit, and are consistent with behavior observed in devices with a hafnium oxide dielectric layer [28].

Conclusions

We report on growth by DC and RF sputtering, of vanadium oxide-on-YSZ structures using different substrates, as well as measurements of the composition and MIT characteristics of these samples. In particular, we demonstrate the RF sputtering of polycrystalline films with a large transition ($\mathcal{R}_{tr} \approx 10^3$) with a hysteresis and transition width of about 7 °C. The distribution of different phases of vanadium oxides in DC-sputtered mixed-oxide films is studied by XPS, and a common tendency for a high surface concentration of oxygen rich phases is identified. Changes in the transition characteristics are examined through a process of low temperature annealing and explained in terms of modifications to the film chemistry deduced from

photoelectron spectra. In particular, over the range of conditions examined, the observed changes in composition are attributed to a relatively lower stability of the VO_2 phase compared to higher and lower oxide phases such as V_2O_5 and V_2O_3 .

Clear resistivity transitions near 70 °C in all the samples described here indicate the suitability of both the substrates and the deposition techniques for future studies of VO_2 /YSZ. C – V measurements performed on Au–Cr/ VO_x /YSZ/ n -Si show an abrupt increase in capacitance in the vicinity of the transition temperature, which is attributed to the MIT in VO_2 .

Acknowledgements The authors would like to thank Yanjie Cui and Kian Kerman for technical assistance as well as Zheng Yang for valuable discussions. We acknowledge NSF supplement PHY-0601184 for financial support. Device fabrication was performed, in part, at the Harvard University Center for Nanoscale Systems (CNS), a member of the National Nanotechnology Infrastructure Network (NNIN) which is supported by NSF Award No. ECS-0335765.

References

1. Berglund CN, Guggenheim HJ (1969) Phys Rev 185:1022
2. Goodenough JB (1971) J Solid State Chem 3:490
3. Morin FJ (1959) Phys Rev Lett 3:34
4. Zylbersztein A, Mott NF (1975) Phys Rev 11:4383
5. Cavalleri A et al. (2001) Phys Rev Lett 87:237401
6. Qazilbash MM et al. (2007) Science 318:1750
7. Sakai J et al. (2008) Phys Rev B 78:033106
8. Stefanovich G et al. (2000) J Phys Condens Matter 12:8837
9. Kim HT et al. (2004) New J Phys 6:52
10. Okimura K, Sakai J (2007) Jpn J Appl Phys 46:813
11. Ko C, Ramanathan S (2008) Appl Phys Lett 93:252101
12. Ruzmetov D et al. (2009) J Appl Phys 106:083702
13. Ruzmetov D et al. (2007) J Appl Phys 102:113715
14. Ruzmetov D et al. (2010) J Appl Phys 107:114516
15. Lee JS et al. (2007) Appl Phys Lett 90:015907
16. Lee JS et al. (2007) Appl Phys Lett 91:133509
17. Gopalakrishnan G et al. (2009) J Mater Sci 44:5345. doi:[10.1007/s10853-009-3442-7](https://doi.org/10.1007/s10853-009-3442-7)
18. Gupta A et al. (2009) Appl Phys Lett 95:111915
19. Chae BG et al. (2004) J Korean Phys Soc 44:884
20. Zhu J, Liu JG (2003) Mater Lett 57:4297
21. Norian KH, Hazell LB (1978) Thin Solid Films 54:L9
22. Krishna MG et al. (1997) Thin Solid Films 312:116
23. Sawatzky GA, Post D (1979) Phys Rev B 20:1546
24. Demeter M et al. (2000) Surf Sci 454:41
25. Youn DH et al. (2004) J Vac Sci Technol A 22:719
26. Youn DH et al. (2004) J Appl Phys 95:1407
27. Yun SJ et al. (2008) Electrochim Solid State Lett 1:H173
28. Yang Z et al. (2010) Phys Rev B 82:205101